

# Gyroton with the Corrugated Resonator

Stanislav Kolosov <sup>1</sup>, Alexander Kurayev <sup>1</sup>, Alexey Rak <sup>1</sup>, Semen Kurkin <sup>2,3,\*</sup> , Artem Badarin <sup>2,3</sup> and Alexander Hramov <sup>2</sup>

<sup>1</sup> Faculty of computer-aided design, Belarusian State University of Informatics and Radioelectronics, Minsk 220013, Belarus; kolosov@bsuir.by (S.K.); kurayev@bsuir.by (A.K.); rak.aliaksei@gmail.com (A.R.)

<sup>2</sup> Institute of Electronic Engineering and Mechanical Engineering, Yuri Gagarin State Technical University of Saratov, Saratov 410054, Russia; badarin.a.a@mail.ru (A.B.); hramovae@gmail.com (A.H.)

<sup>3</sup> Faculty of Nonlinear Processes, Saratov State University, Saratov 410012, Russia

\* Correspondence: kurkinsa@nonlin.sgu.ru; Tel.: +7-8452-998823

Received: 23 November 2018; Accepted: 3 January 2019; Published: 11 January 2019



**Abstract:** A new type of high-power electronic device—a gyroton with a corrugated resonator—is described and investigated. Spatial bunching of the electron beam does not occur in this device, however, highly efficient electron beam power conversion into the rotating electromagnetic field power is possible. The rectilinear electron beam deviates from the axis by the slow  $TM_{11}$  wave, then it gives up longitudinal energy to the same wave with more than 78% efficiency, and an output power up to 30 MW. The developed mathematical model of the interaction of the relativistic electron beam with an irregular circular waveguide and resonator fields presented in this article can be used to calculate and optimize the processes occurring in various microwave electronic devices, such as gyrotrons, gyrotons, TWT, Gyro-TWT, and BWT.

**Keywords:** high-power microwaves; gyroton; irregular waveguide; corrugated resonator; rotating field

## 1. Introduction

Gyrotrons are perspective devices of high-power microwave and plasma electronics. The principle of gyroton operation is presented in the following papers [1–8]. The spatial bunching of electrons does not occur in a gyroton. The initially rectilinear electron beam enters on the center of a revolving asymmetrical TM field, where its circular sweep and beam electron trajectories are congruent, i.e., electron trajectories repeat each other but with the phase shift. This is the fundamental difference between a gyroton and a gyrotron: where the transverse bunching of the spiral electron beam occurs in the usually symmetrical TE fields of a smooth waveguide.

The original idea of a device with revolving fields was proposed by I. Kaufman and G. Oltman in 1965 [9]. This device was called “bermutron”. Later this idea was developed in [10,11], but the device was already named “gyrocon”. Then the basic constructions of devices with the revolving fields were proposed in [1–3]. Later, one of the variants of this device was proposed in [5,12]. This device was called “magnicon” [13,14]. We use the name “gyroton” in this work since this name was already accepted in [3].

Gyrocon and gyroton have distinct designs and mechanisms of electrons interaction with the field of electrodynamic structure. Indeed, gyrocon is the double-cavity amplifier, gyroton—the single-cavity generator. The electron-phasing processes and energy exchange with the electromagnetic field in a gyroton are combined in the single resonator, while these processes are separated and occur in different assemblies in a gyrocon: the beam modulation takes place in the input resonator, the circular sweep—in the space between the first and the second resonators and the extraction of energy—in the gap of the output ring resonator. The energy extraction in a gyrocon occurs in the narrow cavity gap

with the small angle of electrons transit; in a gyroton, inside the cavity on gyroresonance condition. This makes the gyroton a much more promising device in the high-frequency range in comparison with the gyrocon.

The proposed gyroton-generator scheme is shown in Figure 1. The dominant role in operation mechanism of such device plays the  $TM_{11}$  wave which is strongly coupled with the  $TE_{11}$  wave in the corrugated waveguide. The waveguide corrugation leads to the slowdown of the phase velocity along the waveguide. This makes it possible to substantially decrease the required magnetostatic field value to achieve the synchronism between the electron beam and the traveling slow wave.

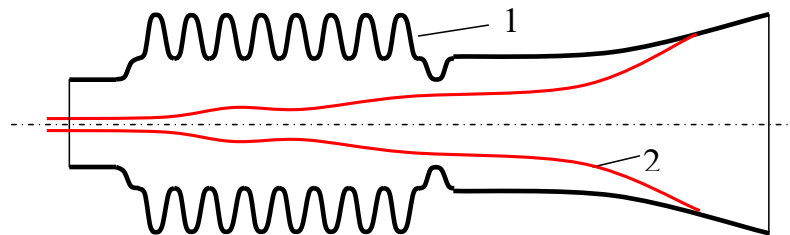


**Figure 1.** The design of the gyroton, here 1 is the profile of the resonator; 2—the electron beam.

A case where the output waveguide is regular was examined in [3]. The development of effective generation process in this modification is possible only in the presence in the system of the magnetostatic field rising to the synchronous value when the regime of the gyroresonance occurs. This leads to strong dependency of generation efficiency on the beam thickness. There is no such dependence in the proposed gyroton, therefore it is possible to reach high efficiencies also for the relatively thick high-power electron beams.

Previously proposed traveling wave gyroton [4] is based on the anomalous Doppler effect [6,15]. The calculated  $TM_{11}$  wave phase velocity is less than the longitudinal velocity of electrons, and the following equation is satisfied

$$1 - \frac{\beta_z}{\beta_w} = -\frac{\Omega_\gamma}{\omega}, \tag{1}$$

here  $\beta_z = \frac{v_z}{c}$ —longitudinal velocity of electrons,  $\beta_w$ — $TM_{11}$  wave phase velocity,  $\Omega_\gamma$ —relativistic cyclotron frequency. Electrodynamic calculation of phase velocity for one corrugation crest for  $TM_{11}$  wave yields the following result in the considered case  $\beta_w = \frac{v_w}{c} = \frac{\Delta\bar{z}}{\Delta\phi_w} = 0.718$  and the longitudinal electrons velocity is  $\beta_z = \frac{v_z}{c} = 0.82$ . The traveling wave gyroton is one of the possible realizations of the maser creation idea based on the anomalous Doppler effect with revolving fields.

In the gyroton with a corrugated resonator, the partial  $TM_{11}$  wave phase velocity ( $\beta_w = \frac{v_w}{c} = 1.7$ ) is greater than the longitudinal electrons velocity. There is a coupled resonator-chain in such gyroton, where the  $TM_{11}$  wave resonates, and the coupling is achieved through the  $TE_{11}$  wave. Therefore, in this case we do not deal with the anomalous Doppler effect. Synchronous regime here is determined by the following condition:

$$1 + \beta_z^2 - \frac{\Omega}{\omega} - \beta_w\beta_z = 0. \tag{2}$$

This equation follows from the equality of the wave phase change and the electron phase change:

$$\omega t - \beta_w\bar{z} = \Omega_\gamma t - \beta_z\bar{z} \tag{3}$$

In traditional gyrotrons the relativistic cyclotron frequency must be approximated to the operating frequency [6,16–18]. So, the gyrotrons advance into range of higher frequencies is limited by the strong magnetostatic fields creation possibility. As it follows from the Equations (1) and (2), gyrotrons can operate at higher frequencies than gyrotrons for the same magnetostatic fields values.

In the corrugated resonator the operating region is sufficiently extended to about 4 wavelengths, while in the cascade gyrotron [3] impact interaction occurs. The corrugated resonator usage makes possible to reduce substantially electric field strength in it.

In References [2,10] only the regime with traveling waves with bimodal approximation is examined. Here, we investigate the standing wave operation regime, taking into account a set of evanescent wave modes. In the corrugated resonator, two traveling towards to each other slow  $TM_{11}$  waves are present, but the wave traveling together with the beam performs the dominant role. In the output waveguide only one  $TE_{11}$  wave propagates and other waves are evanescent. However, the  $TM_{11}$  wave has a primary role in the resonator.

The Figure 2 represents schematically the electron motion in the wave  $TM_{11}$  rotating with the frequency  $\omega$  in the presence of longitudinal magnetostatic field  $H_{z0}$ . Rectilinear electron beam in the waveguide center moves from the z-axis under the action of the  $TM_{11}$  wave magnetic field  $H_t$  and it gains transverse velocity  $V_t$ . Then electrons start to revolve along the Larmor orbit and fall into the  $TM_{11}$  wave phase. As a result,  $E_z$  field of the wave extracts energy from electrons.

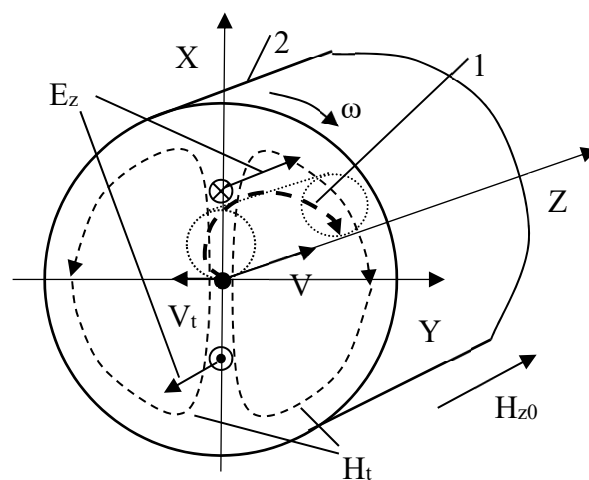


Figure 2. Schematic illustration of the gyrotron waveguide, 1—the electron trajectory; 2—the waveguide.

## 2. Mathematical Model

The mathematical model of the processes occurring in the gyrotron consists of two parts:

- the electromagnetic waves excitation equations in the axisymmetric longitudinally irregular waveguide by a relativistic electron beam;
- the electron beam motion equations in the excited electromagnetic fields.

The irregular waveguide excitation equations were built on the basis of the coordinates transformation method [5,19]. It consists in the substitution of the excitation problem of an irregular waveguide by the excitation of a regular waveguide with the waveguide radius equal to one. This is achieved by the coordinate system replacement. The new coordinate system  $(\rho, \varphi, s)$  is introduced instead of usual polar coordinates  $(r, \varphi, z)$ , using the following equations:

$$\mathbf{a}_\rho = b \cdot \mathbf{r}_0, \mathbf{a}_\varphi = \rho \cdot b \cdot \varphi_0, \mathbf{a}_s = \rho \cdot \frac{\partial b}{\partial z} \cdot \mathbf{r}_0 + z_0, \tag{4}$$

where  $b$  is the internal radius of the waveguide. The contravariant directional vectors system in this case takes the following form:

$$\mathbf{a}^\rho = \frac{1}{b} \cdot r_0 - \frac{\rho}{b} \cdot \frac{\partial b}{\partial z} \cdot z_0, \mathbf{a}^\varphi = \frac{1}{\rho b} \cdot \varphi_0, \mathbf{a}^s = z_0. \tag{5}$$

Maxwell's equations in the new coordinates  $(\rho, \varphi, s)$  in the covariant form are written as follows:

$$\left. \begin{aligned} \text{rot}H' &= \varepsilon_0 \cdot \widehat{g} \cdot \frac{\partial E'}{\partial t} + \widehat{g} \cdot J', \\ \text{rot}E' &= -\mu_0 \cdot \widehat{g} \cdot \frac{\partial H'}{\partial t}. \end{aligned} \right\} \tag{6}$$

The metric tensor into Equation (6) takes the following form:

$$\widehat{g} = \begin{pmatrix} 1 + \rho^2 \cdot \left(\frac{\partial \bar{b}}{\partial z}\right)^2 & 0 & -\rho \cdot \bar{b} \cdot \frac{\partial \bar{b}}{\partial z} \\ 0 & 1 & 0 \\ -\rho \cdot \bar{b} \cdot \frac{\partial \bar{b}}{\partial z} & 0 & \bar{b}^2 \end{pmatrix}, \tag{7}$$

where  $\rho = \frac{r}{b}, \bar{b} = \frac{2\pi b}{\lambda_0}, z = \frac{2\pi Z}{\lambda_0}$ .

Now, expression for the internal waveguide surface in the coordinate system  $(\rho, \varphi, s)$  will take the following form:

$$\rho = 1. \tag{8}$$

The boundary conditions of the waveguide surface in the new coordinate system take the following form:

$$E'_\phi \Big|_{\rho=1} = 0, E'_s \Big|_{\rho=1} = 0. \tag{9}$$

The performed coordinates transformation makes possible to try the wave equations solution in the form of expansions in terms of the regular cylindrical waveguide basic functions. For example, it is possible to search the equations solution (6) for the electrical and magnetic field strengths in the form:

$$\left. \begin{aligned} E'_{1t} &= \text{Re} \sum_m E'_{1tm} \cdot e^{jm\omega t} \\ E'_{1s} &= \text{Re} \sum_m E'_{1sm} \cdot e^{jm\omega t} \end{aligned} \right\} \tag{10}$$

where

$$\left. \begin{aligned} E'_{1tm} &= \sum_{i=1}^I \sum_{n=-N}^N (A_{mni}^E \cdot e_{ni}^E + A_{mni}^M \cdot e_{ni}^M) \\ E'_{1sm} &= \sum_{i=1}^I \sum_{n=-N}^N C'_{mni} \cdot \varphi_{ni} \\ H'_{1m} &= \frac{j}{m\omega\mu_0} \cdot \widehat{g}^{-1} \cdot \text{rot}E'_{1m} \end{aligned} \right\} \tag{11}$$

and the eigenmodes of a regular waveguide are defined as

$$\begin{aligned}
 e_{rni}^E &= J'_n(\nu_{ni}\rho) \cdot e^{-jn\phi}, \\
 e_{\phi ni}^E &= -\frac{jn}{\nu_{ni}\rho} \cdot J_n(\nu_{ni}\rho) \cdot e^{-jn\phi}, \quad e_{rni}^M = -\frac{n}{\mu_{ni}\rho} \cdot J_n(\mu_{ni}\rho) \cdot e^{-jn\phi}, \\
 \phi_{ni} &= J_n(\nu_{ni}\rho) \cdot e^{-jn\phi}, \quad e_{\phi ni}^M = jJ'_n(\mu_{ni}\rho) \cdot e^{-jn\phi}.
 \end{aligned}
 \tag{12}$$

Here  $m$  is the fundamental frequency  $\omega$  harmonic number,  $n$  is the phase index,  $i$  is the radial index,  $j$  is the imaginary value,  $\nu_{ni}$  are the Bessel function roots ( $J_n(\nu_{ni}) = 0$ ), and  $\mu_{ni}$  are the Bessel function derivative roots ( $J'_n(\mu_{ni}) = 0$ ).

The physical vectors  $E, H, J$  are defined via the calculated ones as

$$\left. \begin{aligned}
 E &= E'_\rho \cdot a^1 + E'_\phi \cdot \rho \cdot a^2 + E'_s \cdot a^3, \\
 H &= H'_\rho \cdot a^1 + H'_\phi \cdot \rho \cdot a^2 + H'_s \cdot a^3, \\
 J &= J'_\rho \cdot a^1 + J'_\phi \cdot \rho \cdot a^2 + J'_s \cdot a^3.
 \end{aligned} \right\}
 \tag{13}$$

The Galerkin method was used for solving Maxwell’s equations [5,20]. This method is also called “the method of orthogonalization” and it consists in the fact that the coefficients of expansions (11) are determined from the equations residuals orthogonality condition Equation (6) to the expansion eigenvectors Equation (12) with any s:

$$\begin{aligned}
 &\int_0^{2\pi} \int_0^1 \int_0^{2\pi} \left\{ \text{rot} \left( \widehat{g}^{-1} \cdot \text{rot} E'_1 \right) + \mu_0 \cdot \widehat{g} \cdot \left[ \varepsilon_0 \cdot \frac{\partial^2 E'_1}{\partial t^2} + \frac{\partial J''}{\partial t} \right] \right\}_\perp \cdot e_{ni}^{E,M*} \cdot \rho \cdot d\varphi \cdot d\rho \cdot e^{-im\omega t} \cdot d\omega t = 0, \\
 &\int_0^{2\pi} \int_0^1 \int_0^{2\pi} \left\{ \text{rot} \left( \widehat{g}^{-1} \cdot \text{rot} E'_1 \right) + \mu_0 \cdot \widehat{g} \cdot \left[ \varepsilon_0 \cdot \frac{\partial^2 E'_1}{\partial t^2} + \frac{\partial J''}{\partial t} \right] \right\}_s \cdot \varphi_{ni} \cdot \rho \cdot d\varphi \cdot d\rho \cdot e^{-im\omega t} \cdot d\omega t = 0.
 \end{aligned}
 \tag{14}$$

The expansion coefficients Equation (11) are determined from the Equation (14) by the following ordinary differential equations system:

$$\begin{aligned}
 \frac{dA_{mnp}^e}{dz} &= V_{mnp} + v_{np}C_{mnp} \\
 v_{np}C_{mnp} &= -\frac{V_{mnp}v_{np}^2}{m^2g^2} - \frac{1}{g} \frac{dg}{dz} \frac{v_{np}}{e_{npp}m^2g^2} \sum_i A_{mni}^m \gamma_{npi}^3 + \\
 &\quad \frac{v_{np}}{ge_{npp}} \frac{dg}{dz} \left[ \sum_i A_{mni}^e I_{2nip} - \sum_i A_{mni}^m \bar{\gamma}_{npi}^3 \right] - \\
 &\quad -j \frac{\sigma v_{np}}{me_{npp}\pi g^2} \frac{1}{N_e} \sum_{j=1}^{N_e} J_n(v_{np}\rho_j) e^{-j(n\phi_j - mT_j)} \\
 \frac{dV_{mnp}}{dz} &= -m^2 A_{mnp}^e + \frac{1}{e_{npp}} \sum_i \left\{ \begin{aligned} &A_{mni}^m \left[ -\frac{1}{g^2} \left( \frac{dg}{dz} \right)^2 + \frac{1}{g} \frac{d^2g}{dz^2} \right] + \\ &P_{mni} \frac{1}{g} \frac{dg}{dz} \end{aligned} \right\} \gamma_{npi}^4 + \\
 &\quad -m^2 \left( \frac{dg}{dz} \right)^2 \frac{1}{e_{npp}} \sum_i A_{mni}^e I_{3npi} + m^2 \left( \frac{dg}{dz} \right)^2 \frac{1}{e_{npp}} \sum_i A_{mni}^m \gamma_{npi}^5 + \\
 m^2 g \frac{dg}{dz} \frac{1}{e_{npp}} \sum_i C_{mni} I_{2nip} &- \frac{j m \sigma}{e_{npp} g \pi} \frac{1}{N_e} \sum_{j=1}^{N_e} \left[ \begin{aligned} &\left( \beta_{r_j} - \rho_j \beta_{z_j} \frac{dg}{dz} \right) J'_n(v_{np}\rho_j) + \\ &j \frac{n}{v_{np}\rho_j} J_n(v_{np}\rho_j) \beta_{\phi_j} \end{aligned} \right] \\
 &\frac{e^{j(n\phi_j - mT_j)}}{\beta_{z_j}}
 \end{aligned} \tag{15}$$

$$\begin{aligned}
 \frac{dA_{mnp}^m}{dz} &= P_{mnp} \\
 \frac{dP_{mnp}}{dz} &= -A_{mnp}^m \left[ \begin{aligned} &m^2 \left( 1 + \frac{n^2}{\mu_{np}^2} \left( \frac{dg}{dz} \right)^2 \right) - \frac{\mu_{np}^2}{g^2} - \\ &\frac{\gamma_{snp}^5}{g^2} \left( \frac{dg}{dz} \right)^2 + \frac{1}{g} \frac{d^2g}{dz^2} \gamma_{npi}^6 \end{aligned} \right] + \\
 &\quad + \sum_{i \neq p} A_{mni}^m \left( \left( \frac{1}{g} \frac{dg}{dz} \right)^2 \gamma_{npi}^7 + \frac{1}{g} \frac{d^2g}{dz^2} \gamma_{npi}^8 \right) / h_{npp} + \\
 &\quad \frac{1}{g} \frac{dg}{dz} \sum_{i \neq p} P_{mni} \gamma_{npi}^9 / h_{npp} + \frac{1}{g} \frac{dg}{dz} \sum_i V_{mni} \gamma_{npi}^{10} / h_{npp} + \\
 &\quad + m^2 \left( \frac{dg}{dz} \right)^2 \sum_i A_{mni}^e \gamma_{npi}^5 / h_{npp} - m^2 g \frac{dg}{dz} \sum_i C_{mni} \gamma_{npi}^{12} / h_{npp} - \\
 &\quad -j \frac{m \sigma}{h_{npp} \pi g} \frac{1}{N_e} \sum_{j=1}^{N_e} \left[ \begin{aligned} &-\left( \beta_{r_j} - \rho_j \frac{dg}{dz} \beta_{z_j} \right) \frac{n}{\mu_{np}\rho_j} J_n(\mu_{np}\rho_j) \\ &-j \beta_{\phi_j} J'_n(\mu_{np}\rho_j) \end{aligned} \right] \frac{e^{j(n\phi_j - mT_j)}}{\beta_{z_j}}
 \end{aligned}$$

Here the following designations are accepted:

$$\begin{aligned}
 z &= Z \cdot 2\pi/\lambda_0, g = b \cdot 2\pi/\lambda_0, \beta = V/c, m = \omega/\omega_0, \\
 \sigma &= I_0 \frac{\eta_0 \mu_0}{c} = I_0 \cdot 0.73723 \cdot 10^{-3}, \\
 A_{mnp}^e &= \frac{E_{\perp mnp}^e \eta_0}{c^2}, C_{mnp} = \frac{E_{z mnp}^e \eta_0}{\omega_0 c}, A_{mnp}^m = \frac{E_{\perp mnp}^m \eta_0}{c^2} \\
 \gamma_{npi}^5 &= \frac{2 \cdot n \cdot v_{np}^2}{\mu_{ni} (\mu_{ni}^2 - v_{np}^2)^2} \cdot J_n(\mu_{ni}) \cdot J_{n-1}(v_{np}); \\
 \gamma_{npp}^5 &= \left( \mu_{np}^2 + n^2 \left( 1 - \frac{2n^2}{\mu_{np}^2} + \frac{5}{\mu_{np}^2} \right) \right) \cdot J_n^2(\mu_{np}) / 6; \\
 \gamma_{nip}^6 &= \frac{\mu_{ni} \mu_{np}}{\mu_{ni}^2 - \mu_{np}^2} \left( \frac{n^2}{\mu_{np}^2} - 1 \right) \cdot J_n(\mu_{ni}) \cdot J_n(\mu_{np}); \gamma_{npp}^6 = \frac{n^2}{2\mu_{np}^2} \cdot J_n^2(\mu_{np}); \\
 \gamma_{nip}^7 &= \frac{v_{ni} J_{n-1}(v_{ni}) \cdot J_{n-1}(v_{np})}{v_{ni}^2 - v_{np}^2}; \gamma_{npp}^7 = \frac{e_{npp}}{v_{np}}; \\
 \gamma_{nip}^8 &= \frac{2v_{np}^2}{\mu_{ni}^2 - v_{np}^2} \cdot J_n(\mu_{ni}) \cdot J_{n-1}(v_{np}).
 \end{aligned} \tag{16}$$

The equations system Equation (15) is the longitudinally irregular waveguide excitation by external sources problem solution. In this system, the  $E$  and  $H$  wave modes with the identical azimuthal indices  $n$  are coupled that is caused by the azimuthal waveguide symmetry.

Considering Equations (8), (14) and (15), it is possible to write down the physical vectors of the electromagnetic fields in the following form:

$$\begin{aligned}
 E_{tm} &= E_{xm} + jE_{ym} = \\
 &= \frac{1}{2 \cdot b} \cdot \sum_{i=1}^I \sum_{n=-N}^N \left\{ \begin{aligned} & \left[ \begin{aligned} & A_{mni}^E J_{n-1}(\rho_{Eni}) \cdot e^{-j[(n-1)\varphi - mT]} - A_{mni}^{*E} J_{n+1}(\rho_{Eni}) \cdot \\ & e^{j[(n+1)\varphi - mT]} - A_{mni}^M J_{n-1}(\rho_{Mni}) \cdot e^{-j[(n-1)\varphi - mT]} - \\ & A_{mni}^{*M} J_{n+1}(\rho_{Mni}) \cdot e^{j[(n+1)\varphi - mT]} \end{aligned} \right] \end{aligned} \right\}; \\
 E_{zm} &= \frac{1}{2} \sum_{i=1}^I \sum_{n=-N}^N \left\{ \begin{aligned} & \left[ \begin{aligned} & J_n(\rho_{Eni}) \left[ C_{mni} e^{-j(n\varphi - mT)} + C_{mni}^* e^{j(n\varphi - mT)} \right] - \\ & - \frac{\rho}{b} \cdot \frac{db}{dz} \left[ \begin{aligned} & J'_n(\rho_{Eni}) \left[ A_{mni}^E e^{-j(n\varphi - mT)} + A_{mni}^{*E} e^{j(n\varphi - mT)} \right] - \\ & - \frac{n}{\rho_{Mni}} J_n(\rho_{Mni}) \left[ \begin{aligned} & A_{mni}^M e^{-j(n\varphi - mT)} + \\ & A_{mni}^{*M} e^{j(n\varphi - mT)} \end{aligned} \right] \end{aligned} \right] \end{aligned} \right\}; \\
 H_{tm} &= H_{xm} + jH_{ym} = \\
 &= \frac{1}{2bm\omega\mu_0} \sum_{i=1}^I \sum_{n=-N}^N \left\{ \begin{aligned} & \left[ \begin{aligned} & v_{ni} \left[ \begin{aligned} & C_{mni} J_{n-1}(\rho_{Eni}) e^{-j[(n-1)\varphi - mT]} + \\ & C_{mni}^* J_{n+1}(\rho_{Eni}) e^{j[(n+1)\varphi - mT]} \end{aligned} \right] - \\ & - \frac{dA_{mni}^E}{dz} J_{n-1}(\rho_{Eni}) e^{-j[(n-1)\varphi - mT]} - \\ & \frac{dA_{mni}^{*E}}{dz} J_{n+1}(\rho_{Eni}) e^{j[(n+1)\varphi - mT]} + \\ & + \frac{dA_{mni}^M}{dz} J_{n-1}(\rho_{Mni}) e^{-j[(n-1)\varphi - mT]} - \\ & \frac{dA_{mni}^{*M}}{dz} J_{n+1}(\rho_{Mni}) e^{j[(n+1)\varphi - mT]} + \\ & + \frac{1}{r_b} \cdot \frac{dr_b}{dz} \cdot \rho_{Mni} J_n(\rho_{Mni}) \left[ \begin{aligned} & A_{mni}^M e^{-j[(n-1)\varphi - mT]} + \\ & A_{mni}^{*M} e^{j[(n+1)\varphi - mT]} \end{aligned} \right] \end{aligned} \right] \end{aligned} \right\}; \\
 H_{zm} &= \frac{1}{2bm\omega\mu_0} \sum_{i=1}^I \sum_{n=-N}^N \left\{ \mu_{ni} J_n(\rho_{Mni}) \left[ A_{mni}^M e^{-j(n\varphi - mT)} + A_{mni}^{*M} e^{j(n\varphi - mT)} \right] \right\}.
 \end{aligned} \tag{17}$$

Here  $\rho_{Eni} = v_{ni} \frac{r}{b}$ ;  $\rho_{Mni} = \mu_{ni} \frac{r}{b}$ .

The motion equations of the  $i$ -th charged particle in the irregular waveguide electromagnetic field in the heterogeneous magnetostatic field take the form:

$$\left. \begin{aligned} \frac{d\beta_{xi}}{dz} &= -\frac{R_i}{\beta_{zi}} [\bar{E}_{xi} + \beta_{yi}F - \beta_{zi}(\bar{H}_{yi} + F_{yi}) - \beta_{xi}(\beta_{xi}\bar{E}_{xi} + \beta_{yi}\bar{E}_{yi} + \beta_{zi}\bar{E}_{zi})], \\ \frac{d\beta_{yi}}{dz} &= -\frac{R_i}{\beta_{zi}} [\bar{E}_{yi} - \beta_{xi}F + \beta_{zi}(\bar{H}_{xi} + F_{xi}) - \beta_{yi}(\beta_{xi}\bar{E}_{xi} + \beta_{yi}\bar{E}_{yi} + \beta_{zi}\bar{E}_{zi})], \\ \frac{d\beta_{zi}}{dz} &= -\frac{R_i}{\beta_{zi}} [\bar{E}_{zi} + \beta_{xi}(\bar{H}_{yi} + F_{yi}) - \beta_{yi}(\bar{H}_{xi} + F_{xi}) - \\ &\beta_{zi}[\beta_{zxi}\bar{E}_{xi} + \beta_{zyi}\bar{E}_{yi} + \beta_{zzi}\bar{E}_{zi}]], \\ \frac{dx_i}{dz} &= \beta_{xi}/\beta_{zi}, \frac{dy_i}{dz} = \beta_{yi}/\beta_{zi}, \frac{dT_i}{dz} = 1/\beta_{zi} \end{aligned} \right\} \quad (18)$$

Here the following designations are accepted:

$$\begin{aligned} R_i &= \sqrt{1 - \beta_{xi}^2 - \beta_{yi}^2 - \beta_{zi}^2}, F(z) = \frac{\mu_0 e H_z^0(z)}{\omega_0}, \\ F_{xi} &= -\frac{r_i}{2} \frac{dF}{dz} \cos \varphi_i, F_{yi} = -\frac{r_i}{2} \frac{dF}{dz} \sin \varphi_i, \\ r_i &= \sqrt{x_i^2 + y_i^2}, \varphi_i = \arctan(y_i/x_i), \\ \bar{E}_{xi} + j\bar{E}_{yi} &= \frac{\eta_0}{\omega_0 c} (E_{xi} + jE_{yi}), \bar{E}_{zi} = \frac{\eta_0}{\omega_0 c} E_{zi}, \\ \bar{H}_{xi} + j\bar{H}_{yi} &= \frac{\eta_0 \mu_0}{\omega_0} (H_{xi} + jH_{yi}), \bar{H}_{zi} = \frac{\eta_0 \mu_0}{\omega_0} H_{zi}. \end{aligned} \quad (19)$$

Initial conditions for the system of Equations (15) in the electron beam initial modulation absence can be defined in the following form:

$$\left. \begin{aligned} \phi_i(0) &= \frac{2\pi}{N}(i-1), \beta_{xi} = -\beta_{\perp 0} \sin \phi_i(0), \\ \beta_{yi}(0) &= \beta_{\perp 0} \cos \phi_i(0), \beta_{zi}(0) = \beta_{z0}, \\ \beta_{z0} &= \beta_0 / \sqrt{1+q^2}, \beta_{\perp 0} = \beta_{z0}q; \\ x_i(0) &= r_{vc} + \beta_{\perp 0} / (F(0)R_0) \cos \phi_i, \\ y_i(0) &= \beta_{\perp 0} / (F(0)R_0) \sin \phi_i, \\ T_i &= 0 \end{aligned} \right\}. \quad (20)$$

where  $N$ —the electrons number,  $\beta_0 = \frac{v_0}{c}$ —normalized initial electrons velocity,  $R_0 = \sqrt{1 - \beta_0^2}$ ,  $r_{vc}$ —normalized radius of the electrons Larmor orbit center,  $q = \frac{v_{\perp}}{v_{\parallel}}$ —ratio of the electrons transverse velocity to the longitudinal velocity.

The electronic efficiency is defined as

$$\eta_e(z) = \frac{1}{N} \sum_{i=0}^N \frac{1 - R_0/R_i(z)}{1 - R_0}. \quad (21)$$

### 3. Algorithm and Calculations Results

The method proposed in this article reduces the 3D task to 1D. It increases considerably both speed and accuracy of boundary-value problem solution. The known codes MAGIC [21], CST [22], KARAT [23], and MAGY [24] etc. do not have such convergence speed of boundary-value problems solution, and this makes it impossible to solve the optimization problem of the gyrotron waveguide profile in the acceptable calculating time.

The Cauchy problem direct solution for the electrons motion equations system and waves excitation in an irregular waveguide by the usual integration methods (for example, the Runge-Kutta method) is impossible when evanescent modes are taken into account. The equations system is very unstable in this case. The method of block matrix dispersion was used to solve the boundary-value problem [25].

Own software package CEDR (complex of electrodynamic resolutions) [26], that was developed for mathematical simulation and optimization of the nonlinear and linear processes of relativistic electron beam interaction with the irregular electrodynamic systems fields, has been used in our work for the calculations in spectral domain, i.e., we have investigated the steady-state regime. We have applied the module GYRO-K of the package CEDR. The self-consistent nonlinear problem has been solved. The starting current has been determined asymptotically by decreasing current from the working value to the value when efficiency of the device was close to zero. We have determined the amplitude characteristic at the same time. The analysis of it indicates stability of the generation excitation process in the device. The detailed investigations that were conducted in the work [27] confirm the generation process stability in a gyrotron.

The search for the gyrotron optimal construction with corrugated resonator with the help of the described program has yielded the following result: accelerating voltage  $V_0 = 381$  kV, beam current  $I_0 = 8.7$  A, resonator length  $l = 2\pi L/\lambda_0 = 25$ , corrugation internal radius  $g_1 = 2\pi r_1/\lambda_0 = 2.902$ , corrugation amplitude  $\Delta g = 2\pi\Delta r/\lambda_0 = 2.05$ , the output ridge radius  $g_3 = 1.902$ , the corrugation edges number  $n = 14$ , the magnetostatic field value  $F = H/H_s = 1.113$ .

Only one  $TE_{11}$  wave propagates in the output waveguide. The corrugation cavities form five coupled double-humped resonators operating mostly on  $TM_{11}$  wave. In total, 16 wave modes were considered in the calculations: eight waves  $TM_{11}$ – $TM_{18}$  and eight waves  $TE_{11}$ – $TE_{18}$ . The obtained results were verified by increasing the calculations accuracy: the waveguide base functions number was varied from 16 to 64 and the integration steps number—from 2000 to 8000. The accuracy change did not exceed 1% in this case.

As it follows from Figure 3, the largest amplitude has  $TM_{11}$  wave. The electronic efficiency of this gyrotron reaches 78%. The resonator profile is corrugated, and it is connected at the left side with the drift tube that is below-cutoff for all the wave modes (at the operating frequency); the rectilinear electron beam is injected through this tube center. To the right, the corrugation ends with the internal contraction, which increases the quality of this resonator.

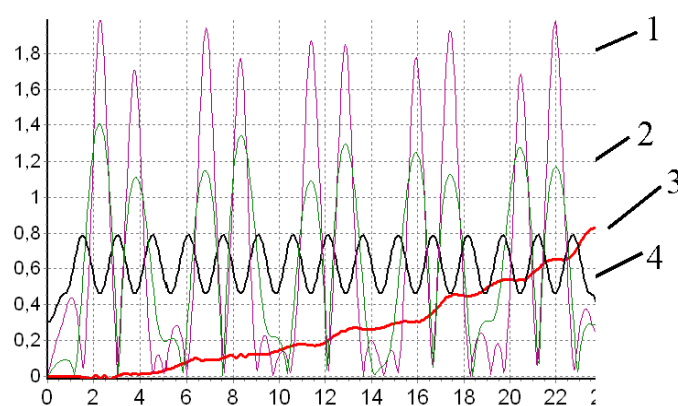


**Figure 3.** Fields distributions of the modes in the resonator. Curve 1 corresponds to the wave amplitude for  $TM_{11}$  mode; 2—the wave amplitude for  $TE_{11}$  mode; 3—the dependence of efficiency on longitudinal coordinate  $z$ ; 4—the profile of the resonator  $b(z)/\lambda_0$ .

The frequency characteristics of the squared amplitude of the overall waves for the main resonance in this resonator at a constant power of the wave  $TM_{11}$  falling to the right is presented in Figure 4. Figure 4 shows that the resonator cold Q-factor is  $Q_n = 5250$ . Therefore, the field in this construction of gyrotron can be considered as fixed with a high degree of accuracy.

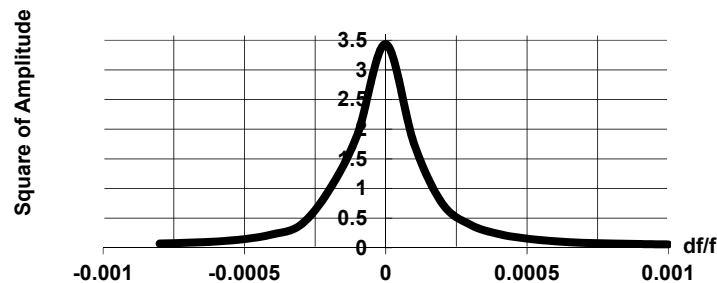


Figure 4. Frequency characteristic of the main resonance of the corrugated resonator.

Figure 5 demonstrates the gyrotron integral characteristics. One can see that the electron beam deviates initially from the axis by the transverse component of the rotating  $TM_{11}$  wave high-frequency magnetic field. The electrons gyration radius and the rotation leading center radius increase simultaneously in this case (curves 4 and 6), this means that the electrons orbits only touch upon the resonator axis. Consequently, beginning with  $z > 3$ , the electron beam begins to give up its longitudinal energy to the longitudinal electrical component of the  $TM_{11}$  wave (curve 2). The efficiency increases almost monotonically with the growth of  $z$  (curve 1), and the electron’s rotation center radial coordinate gradually moves away from the device axis (curve 4). So, device high efficiency is achieved only due to use of the electrons longitudinal energy.

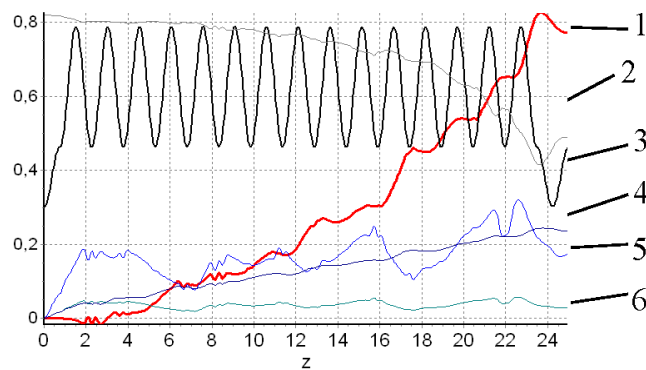


Figure 5. Integral characteristics of the gyrotron: curve 1 corresponds to the dependence of efficiency on longitudinal coordinate  $z$ ; 2—the longitudinal electrons velocity  $\beta_z = v_z/c$ ; 3—the resonator profile  $g = b/\lambda_0$ ; 4—the electrons rotation center radius; 5—the electrons transverse speed  $\beta_t = v_t/c$ ; 6—the electrons gyration radius  $r_e/\lambda_0$ .

The internal ridge at the end of the resonator increases the resonator Q-factor up to 5250, which makes it possible to reduce the device operating current to 8.7 A. The linear estimation of the start-oscillation current is 6.7 A. However, it also limits the thickness of the electron beam to  $2\pi D/\lambda \leq 1$ . At the higher thicknesses the beam begins to deposit on this ridge. The reduction in the efficiency with the increase of the beam radius is shown in Figure 6.

The resonator frequency characteristics study in a broad band ( $\sim 10\%$ ) has been carried out. The frequency characteristic for the squared amplitude of the overall waves in the resonator in 10%-band of frequencies is presented in Figure 7. Several resonances can be seen at the frequencies both lower and higher relative to the main resonance frequency.

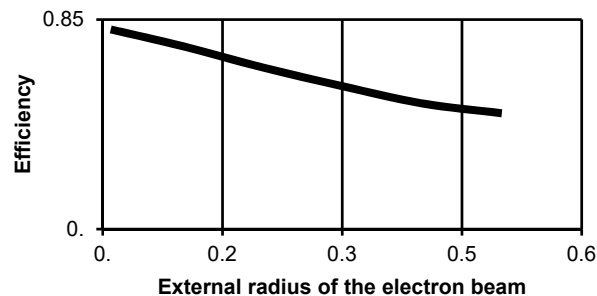


Figure 6. Influence of radius of the electron beam on device efficiency.

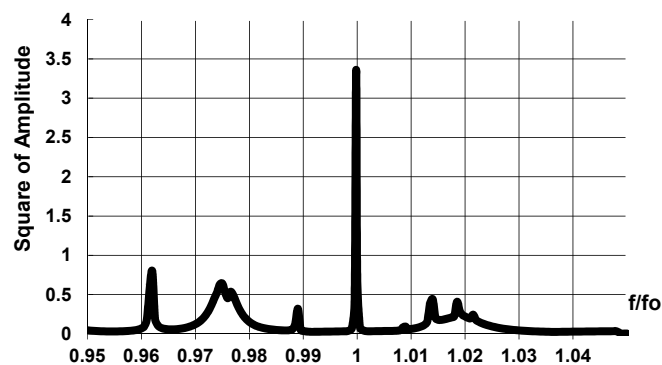


Figure 7. The frequency characteristic of the corrugated resonator.

As follows from Figure 7, all existing resonances except for the main one possess lower diffraction quality and they cannot influence to the electron beam in the same manner as the main resonance.

#### 4. Discussion and Conclusions

The gyrotron-generator with the corrugated resonator can operate with efficiency about 78% and output power  $\sim 2.6$  MW. If we increase the inside radius of the waveguide to the cut-off value for the  $TM_{11}$  wave, then it is possible to substantially lower the resonator quality and it is, respectively, essential for the increasing of the gyrotrons output power. The mathematical model of the relativistic electron beam interaction processes with the irregular circular waveguides and resonators fields presented in this paper can be used for the calculation and optimization of the processes occurring in various microwave electronic devices, such as gyrotrons, gyrotrons, BWOs, and TWTs.

**Author Contributions:** Conceptualization, S.K. and A.K.; Methodology, A.K. and A.H.; Software, A.B. and S.K.; Validation, A.B., A.R. and S.K.; Formal Analysis, A.R.; Investigation, S.K.; Data Curation, A.K.; Writing—Original Draft Preparation, S.K.; Writing—Review & Editing, S.K.; Visualization, A.R.; Supervision, A.K.; Project Administration, S.K.

**Funding:** This work has been supported by the Russian Foundation for Basic Research (18-32-20135), the Ministry of Education and Science of the Russian Federation (3.859.2017/4.6).

**Conflicts of Interest:** The authors declare no conflict of interest.

## References

1. Kolosov, S.V.; Kurayev, A.A. Nonlinear radiation and conversion of longitudinal energy of relativistic electronic beam in the strong revolving electromagnetic fields. *J. Commun. Technol. Electron.* **1973**, *18*, 2558–2566.
2. Kurayev, A.A. To design the amplifier on relativistic electron beam with magnetic modulator. *J. Commun. Technol. Electron* **1982**, *27*, 1231–1234.
3. Kurayev, A.A.; Sinitsyn, A.K.; Slepyan, A.Y. Gyroton. *Int. J. Electron.* **1996**, *80*, 603–610. [[CrossRef](#)]
4. Kolosov, S.V.; Kurayev, A.A.; Lavrenov, A.A. Traveling wave gyroton with double mode operations. In Proceedings of the Third IEEE International Vacuum Electronics Conference (IVEC-2002), Monterey, CA, USA, 23–25 April 2002; pp. 115–116.
5. Nezhevenko, O.A. Gyrocons and Magnicons: Microwave Generators with Circular Deflection of the Electron Beam. *IEEE Trans. Plasma Sci.* **1994**, *22*, 756–772. [[CrossRef](#)]
6. Bratman, V.L.; Ginzburg, N.S.; Nusinovich, G.S.; Petelin, M.I.; Yulpatov, V.K. *Cyclotron and Synchrotron Masers. Relativistic UHF Electronics*; IAP, Gorky: Nizhni Novgorod, Russia, 1979; Volume 1, pp. 141–162.
7. Kolosov, S.V.; Kurayev, A.A. Nonlinear theory of gyroresonance devices with the irregular electrodynamic system. *Electromagn. Waves Electron. Syst.* **1998**, *3*, 35–44.
8. Qiu, C.R.; Ouyang, Z.B.; Zhang, S.C.; Zhang, H.B.; Jin, J.B. Self-consistent nonlinear investigation of an outer-slotted-coaxial waveguide gyroton traveling-wave amplifier. *IEEE Trans. Plasma Sci.* **2005**, *33*, 1013–1018.
9. Kaufman, I.; Oltman, G. Harmonic Generation by Electron Beam Pattern Motion—The Bermutron. *IEEE Trans. Electron Devices* **1965**, *12*, 31–39. [[CrossRef](#)]
10. Budker, G.I.; Karliner, M.M.; Makarov, I.G.; Morozov, S.N.; Nezhevenko, O.A.; Ostreiko, G.N.; Shekhtman, I.A. Microwave Electron Discharge Device. U.S. Patent No. 3,885.193, 20 May 1975.
11. Budker, G.I.; Karliner, M.M.; Makarov, I.G. The Gyrocon: An Efficient Relativistic High-Power VHF generator. *Sov. At. Energy* **1978**, *44*, 459–466. [[CrossRef](#)]
12. Karliner, M.M.; Kozyrev, E.V.; Maksimov, A.Y.; Nezhevenko, O.A.; Ostrenko, G.N. *Electron Device—Magnicon, Certificate of Authorship #SU 1110335 A Moscow, Russia, 1986*. Available online: <http://patents.su/4-1110335-ehlektronnyj-pribor-svch-magnikon.html> (accessed on 22 December 2018).
13. Gold, S.H.; Fliflet, A.W.; Hafizi, B.; Gordon, D.F.; Kinkead, A.K. Transient Effects in an X-Band Magnicon Amplifier. *IEEE Trans. Plasma Sci.* **2010**, *38*, 1329–1336. [[CrossRef](#)]
14. Nezhevenko, O.A.; LaPointe, M.A.; Yakovlev, V.P.; Hirshfield, J.L. Commissioning of the 34-GHz, 45-MW pulsed magnicon. *IEEE Trans. Plasma Sci.* **2004**, *32*, 994–1001. [[CrossRef](#)]
15. Nusinovich, G.S.; Zhao, D. Combined Resonances in Cyclotron Masers with Periodic Slow-Wave Structures. *IEEE Trans. Plasma Sci.* **2015**, *43*, 804–814. [[CrossRef](#)]
16. Du, C.H.; Qi, X.B.; Liu, P.K.; Chang, T.H.; Xu, S.X.; Geng, Z.H.; Hao, B.L.; Xiao, L.; Liu, G.F.; Li, Z.D.; Shi, S.H. Theory and Experiment of a W-Band Tunable Gyrotron Oscillator. *IEEE Trans. Electron Devices* **2014**, *61*, 1781–1788. [[CrossRef](#)]
17. Qin, M.; Luo, Y.; Yang, K.; Huang, Y.; Li, H.; Wang, S. Nonlinear Theory of a Corrugated Coaxial- Gyrotron With Misaligned Inner Rod. *IEEE Trans. Electron Devices* **2014**, *61*, 4247–4252. [[CrossRef](#)]
18. Bratman, V.L.; Kalynov, Y.K.; Kalynova, G.I.; Manuilov, V.N.; Makhlov, P.B. Frequency Tuning in a Subterahertz Gyrotron With a Variable Cavity. *IEEE Trans. Electron Devices* **2014**, *61*, 3529–3533. [[CrossRef](#)]
19. Kurayev, A.A.; Popkova, T.L.; Rak, A.O. Excitation equations for the arbitrarily-irregular coaxial waveguide. In Proceedings of the 12th IEEE International Vacuum Electronics Conference (IVEC-2011), Bangalore, India, 21–24 February 2011; p. 353.
20. Stock, A.; Neudorfer, J.; Riedlinger, M.; Pirrung, G.; Gassner, G.; Schneider, R.; Roller, S.; Munz, C.D. Three-Dimensional Numerical Simulation of a 30-GHz Gyrotron Resonator with an Explicit High-Order Discontinuous-Galerkin-Based Parallel Particle-In-Cell Method. *IEEE Trans. Plasma Sci.* **2012**, *40*, 1860–1870. [[CrossRef](#)]
21. Goplen, B.; Ludeking, L.; Smith, D.; Warren, G. User-configurable MAGIC for electromagnetic PIC calculations. *Comput. Phys. Commun.* **1995**, *87*, 54–86. [[CrossRef](#)]
22. CST AG. *User Manual, CST PS*; CST AG: Darmstadt, Germany, 2011.
23. Tarakanov, V.P. *User's Manual for Code KARAT*; Berkley Research Associates, Inc.: Springfield, VA, USA, 1992.

24. Betton, M.; Antonsen, T.M.; Levush, B.; Nguyen, K.T.; Vlasov, A.N. MAGY: A time-dependent code for simulation of slow and fast microwave devices. *IEEE Trans. Plasma Sci.* **1998**, *26*, 882–892. [[CrossRef](#)]
25. Kravchenko, V.F.; Kurayev, A.A.; Pustovoit, V.I.; Sinitsyn, A.K. Irregular waveguide in UHF electronics. *Electromagn. Waves Electron. Syst.* **2005**, *10*, 51–58.
26. Kolosov, S.V.; Kurayev, A.A.; Senko, A.V. The simulation code CEDR. In Proceedings of the 11th IEEE International Vacuum Electronics Conference (IVEC-2010), Monterey, CA, USA, 18–20 May 2010; p. 115.
27. Kravchenko, V.F.; Kurayev, A.A.; Sinitsyn, A.K. Nonsynchronous interactions. *Phys. Uspekhi* **2007**, *50*, 489. [[CrossRef](#)]



© 2019 by the authors. Licensee MDPI, Basel, Switzerland. This article is an open access article distributed under the terms and conditions of the Creative Commons Attribution (CC BY) license (<http://creativecommons.org/licenses/by/4.0/>).